Title
ELASTIC PROTON-PROTON SCATTERING AT 2.24, 4.40, AND 6.15 Bev

Authors
Cork, Bruce
Wenzel, William A.
Causey, Charles W.

Publication Date
1957-04-08

UNIVERSITY OF CALIFORNIA

Radiation Laboratory

BERKELEY, CALIFORNIA

DISCLAIMER

UCRL-3750

UNIVERSITY OF CALIFORNIA
Radiation Laboratory
Berkeley, California

Contract No. W-7405-eng-48

ELASTIC PROTON-PROTON SCATTERING AT 2.24, 4.40, AND 6.15 Bev

Bruce Cork and William A. Wenzel
and
Charles W. Causey, Jr.
U. S. Naval Postgraduate School
Monterey, California

April 8, 1957

Printed for the U. S. Atomic Energy Commission

ELASTIC PROTON-PROTON SCATTERING AT 2.24, 4.40, AND 6.15 Bev

Bruce Cork and William A. Wenzel

Radiation Laboratory
University of California
Berkeley, California

and

Charles W. Causey, Jr.

U. S. Naval Postgraduate School
Monterey, California

April 8, 1957

ABSTRACT

Protons of the internal circulating beam of the Bevatron were scattered in a polyethylene target. Both scattered and recoil protons were detected by scintillation counters at angles which define elastic proton-proton events. An internal counter was located within a few inches of the beam to permit measurements at laboratory scattering angles as low as 2°. Absolute values are based on the calibration of the induction electrode that monitors the circulating beam. Total elastic cross sections obtained by integrating the differential spectra are 17, 10, and 8 mb at 2.24, 4.40, and 6.15 Bev, respectively. The experimental angular distributions are consistent with the prediction of a simple optical model with a complex index of refraction at short range.

ELASTIC PROTON-PROTON SCATTERING AT 2.24, 4.40, AND 6.15 Bev*

Bruce Cork and William A. Wenzel

Radiation Laboratory
University of California
Berkeley, California

and

Charles W. Causey, Jr.

U. S. Naval Postgraduate School
Monterey, California

April 8, 1957

INTRODUCTION

Measurements of nucleon-nucleon scattering cross sections have been of great importance in the investigation of nuclear forces. The results of experiments at bombarding energies below about 300 Mev indicate that the forces between nucleons are attractive at ranges $\gtrsim 10^{-13}$ cm but that a strong repulsive force exists between nucleons when their separation is somewhat less than 10^{-13} cm. As the bombarding energy is increased above the threshold for meson production (290 Mev) to about 800 Mev, the inelastic p-p scattering cross section[1,2] rises while the elastic cross section remains nearly constant.[2] The angular distribution, nearly isotropic at energies below about 400 Mev, exhibits forward peaking, reflecting the inelastic processes that occur within a region of radius larger than the wave length of the colliding particles.

Rarita and Serber[3] have shown that the differential elastic cross-section measurements by Smith, McReynolds, and Snow and the total cross-section measurements by Chen, Leavitt, and Shapiro[1] for bombarding protons of 1 Bev are described fairly well by a "black sphere" interaction, although a detailed phase-shift analysis by Rarita[4] shows that the interaction is certainly considerably more complicated. Recent measurements[5,6] made with cloud chambers indicate that the inelastic p-p cross section is about constant at 26 mb for bombarding energies from 1 to 5 Bev, and that the elastic cross section at 3 Bev is somewhat less than at 1 Bev.

In order to obtain more detailed information about the structure of the nucleon and the interactions between nucleons, detailed angular distributions

---

*Work done under the auspices of the U. S. Atomic Energy Commission.

at the high energies are needed. In this report we describe the measurement of the angular distribution of the elastic scattering at each of three Bevatron energies.

I. EXPERIMENTAL PROCEDURE

A. Proton Beam

The source of bombarding protons is the circulating beam of the Bevatron. The magnitude of the beam is measured by an induction-electrode monitor. The energy is determined by the value of the magnetic field and the radius at which the beam strikes the target. The average energy is known to within 1%. In order to reduce pile-up in the electronics, the beam is spilled onto the target for a period of 10 to 100 milliseconds. This introduces an energy spread in the beam amounting to about 4 Mev per millisecond.

B. Targets

The target of polyethylene or carbon was located in the upstream end of the west straight section of the Bevatron (Fig. 1). Either of two locations was used, depending on the scattering angle. Because the entire aperture of the Bevatron is filled with beam at injection, the target was dropped about 6 inches into the center of the aperture only after the beam had been accelerated to the desired energy. The beam, which had been tracked at a radius outside the target position, was then spilled slowly onto the target. Actual movement of the target was accomplished by a rotary solenoid synchronized with respect to the Bevatron acceleration cycle. In order to minimize background, one or two nylon threads were used to lower the target. Figure 2 shows the targets used in various parts of the experiment. The target illustrated in Fig. 2-A is a 1/2-inch-high by 1/2-inch-diameter cylinder suspended on a single thread. This was used in measurements at angles large enough so that both "scattered" and "recoil" proton could escape easily without serious scattering. A carbon cylinder could be substituted to check the background due to events in the carbon of the CH_2 target. The target of Fig. 2-B, 1/2-by-3/2-by-1/16-inch polyethylene, was used for small-angle scattering where the "recoil" proton has more trouble escaping from the target. To maintain proper orientation with respect to the beam, two threads were required for support. Fig. 2-C shows a 3-by-1-by-1-inch polyethylene target with a 1-by-1/2-by-1/4-inch

"lip." The function of the "lip" in reducing betatron oscillations of the beam has been described by McMillan.[7] This "thick" target was used to calibrate at each energy the external beam monitor (Fig. 1), a two-counter telescope, which detected charged particles emitted at 50° from the target.

C. Counters

Protons elastically scattered from protons in the target were detected by scintillation counters. Each counter consisted of a plastic scintillator viewed by an RCA 1P21 photomultiplier with a lucite light pipe. Counters were located in the plane of the beam orbit both inside and outside of the beam centerline, so that both particles from a given proton-proton scattering event were detected. Protons scattered outward at laboratory angles of 10° to 40° (Fig. 1) were detected by a two-counter telescope located outside a thin window (0.060-inch aluminum) in the outside of the Bevatron straight section. The front scintillator of this telescope defines an aperture 3 inches high and 1 inch wide. For laboratory scattering angles less than 10° a single counter (Fig. 1) inside the Bevatron straight section was used. This counter could be rotated into position while protons were being accelerated in the Bevatron. In this way the aperture could be left free at injection, but the scintillator could be located within a few inches of the beam line after acceleration. Rotation was accomplished by a solenoid-operated compressed air cylinder. The photomultiplier was well shielded for operation in a peak field of 1500 gauss. The counter was operated at atmospheric pressure. The vacuum seal was made on the outside of the rotating tube which moved the scintillator through 90° into the horizontal plane of the beam. The scintillator as seen from the target, was 1/2 inch wide by 2 inches high by 1/4 inch thick.

The protons emitted at large angle ("recoil" protons) were detected by a two-counter telescope. These protons emerged from a thin window (0.020-inch aluminum) on the inside of the straight section at angles of from about 35° to 90° from the target. The aperture defined by the front counter of this telescope was 1 by 1 inch as seen from the target. The front scintillator was 1/8 inch thick, thin enough to pass relatively low-energy protons. The rear counter was large enough (2-3/4-inch diameter) to catch low-energy protons scattered in the front counter. This telescope was mounted on a four-wheel cart which could be driven in the horizontal plane by a remote-controlled selsyn along a rack with a 66-inch radius of curvature about the target position.

A 2-counter telescope 24 feet from the target at 50° to the beam was used as a secondary monitor. Each counter consisted of a plastic scintillator with lucite light pipe, viewed by an RCA 6199 photomultiplier. After calibration against the circulating beam monitor, this telescope served to measure the flux of protons striking the target.

D. Electronics

A block diagram of the electronics is shown in Fig. 3. The signal from each 1P21 is amplified by Hewlett-Packard 460-A distributed amplifiers and fed with proper timing into each of two fast-coincidence circuits. These were either threefold or fourfold depending upon whether the outside telescope or the single-flip counter was used to detect the forward scattered proton. The resolving time was ordinarily set at about ± 3 millimicroseconds. A coincidence occurred if particles went through both inside and outside counters with the timing corresponding to an elastic proton-proton event. The output of each coincidence circuit, after further amplification, operated a fast discriminator and was recorded on a Hewlett-Packard 10 Mc prescaler followed by a UCRL scale-of-1000 scaler.

After careful balancing of the two coincidence circuits, the delay of the inputs from the inside counters to one of the circuits was changed by 10^{-8} sec. This detuned circuit then recorded only accidental coincidences, and provided a continual correction for accidental coincidences observed in the other circuit.

Simultaneously, coincidences in the monitor telescope were recorded on another scaler.

E. Scattering Measurements

The interaction of protons with matter at high energies is largely inelastic. For this reason and because a polyethylene target contains relatively little hydrogen, the number of elastic proton-proton events measured was very small compared with the total number of particles detected by each of the scintillation counters. The size of the counters was dictated largely by the geometry of the Bevatron tangent tank where the experiment was performed and the need for "good" geometry conditions at all times. Minimum counter size was set by target and counter alignment requirements. With the chosen scintillator area of the order of a square inch, the singles counting rate reached

the maximum tolerable level of about 10^4 per pulse when the circulating beam level was about 10^8 protons per Bevatron pulse.

With the need for keeping the counter area small under a wide variety of conditions under varying scattering angles, a somewhat unusual method was used to determine the solid angle subtended by the counters at the target.

The laboratory solid angle is given by the expression

$$\Delta\Omega = \Delta\theta\Delta\phi \sin\theta , \qquad (1)$$

where θ is the polar angle (or in this case the scattering angle) and $\Delta\theta$ and $\Delta\phi$ are respectively the differential polar and azimuthal angles subtended by the defining counters. In our case $\Delta\phi$ was set by the inside (large-angle) defining counter. In fact, we have $\Delta\phi = h_i/\rho_i$ and $\Delta\theta = w_o/r_o$, where w and h are horizontal width and vertical height, respectively, of the counters, ρ is the perpendicular distance from counter to beam line, r is the distance from target to counter, and subscripts o and i refer to outside and inside counter, respectively. Since we have $\rho_i = r_i \sin\theta_i$, Eq. (1) becomes

$$\Delta\Omega = \frac{h_i\, w_o \sin\theta_o}{r_i\, r_o \sin\theta_i} . \qquad (2)$$

For each counter the dimension that did not define the solid angle was large enough to accommodate all events that fell within the corresponding dimension of the other counter, with allowance for finite target size, misalignment, and multiple Coulomb scattering. This condition was readily achieved in the vertical direction, since kinematically $\Delta\phi_i = \Delta\phi_o$ and the inside counters are in every case further from the beam line than the outside counters. The target is 0.5 inch high, Δh_i = 1 inch, so that Δh_o = 3 inches (or 2 inches in the case of the internal rotating counter) is adequate. In the horizontal plane, the situation is complicated because for small-angle scattering we have $\Delta\theta_i > \Delta\theta_o$. Therefore, in the making of measurements, the inside counter is scanned in angle by remote control. The resultant angular spectrum of counts must be integrated to obtain the yield that corresponds to the solid angle given by Eq. (2). This procedure has several advantages. The use of "good" geometry permits separation of elastic proton-proton scattering from other events, such as quasi-elastic scattering from the carbon in the target, or many-body events, which occasionally may produce two particles in directions that correspond to an elastic proton-proton event. Such background is roughly independent

of angle and can easily be subtracted in the angular spectrum obtained. In the same way any electronic mismatch between the coincidence circuits appears as a constant background (positive or negative).

Figure 4 shows the angular spectrum obtained at 6.15 Bev for a laboratory-system scattering angle of 5°. Data obtained with a pure carbon target also are indicated. There is apparently no background from the carbon of the target. Figure 5 is a similar spectrum obtained for a scattering angle of 3°. Carbon background is not shown.

F. Absolute Calibration

The importance of keeping counter geometry "good" and the fact that low-energy (recoil) protons must escape from the target without serious multiple Coulomb scattering require that the target be "thin" during the runs when the scattering measurements are made. Under these conditions, however, each particle of the circulating beam makes (on the average) many traversals through the target. An accurate estimate of this effect is complicated by attenuation, multiple scattering, and beam dynamics in the magnetic field of the Bevatron. Since the yield of scattered events is proportional to the number of beam traversals of the target, an absolute measurement of the scattering cross section requires a determination of this effect. In this experiment the use of a counter telescope as a secondary monitor postpones to a separate experiment the problem of absolute calibration. The yield of elastically scattered protons N_{pp} into a solid angle $\Delta\Omega$ from a thin target containing n protons per square centimeter is $N_{pp} = nN(d\sigma/d\Omega)\Delta\Omega$, where N is the number of incident protons and $d\sigma/d\Omega$ is the cross section per unit solid angle for an elastic p-p collision. From a target of the same material the number N_m of charged particles that are detected by a monitor telescope at a fixed location with respect to the target is $N_m = KnN$, where K is a constant except for a dependence on the energy of the beam. Hence, the monitor telescope serves as a convenient reference for obtaining relative cross sections for different angles at the same energy. To obtain absolute values K must be measured. This is done with the use of a polyethylene target (Fig. 2-C) thick enough so that N may be made exactly equal to the number of protons in the circulating beam. The idea is as follows.

The Bevatron beam circulating outside the target is steered into the lip. After a few passes through the lip the betatron oscillations are damped out, and the beam moves onto the target proper. A single pass through 3 inches

of polyethyiene causes the beam to lose so much energy that the equilibrium orbit is displaced to smaller radius by several inches. As it executes betatron oscillations about this new equilibrium orbit, the beam swings to its innermost radius approximately on the opposite side of the Bevatron from the target. Here a clipper consisting of a copper block several inches thick is plunged into the aperture from the inside radius to within a few inches of the target radius. This clipper intercepts those circulating protons which have passed through the target once.

Because of multiple scattering in the lip and the small amount of the orbit displacement per lip traversal, grazing passes through the target proper may occur. Particles that pass through less than the full target thickness produce on the average fewer monitor counts, and their orbits are displaced relatively less. Hence the monitor yield per circulating proton is a function of the radius to which the clipper is plunged. This effect is shown in Fig. 6 for each of the three energies measured. The width of the "plateau" in each case is in good agreement with the prediction based on the calculated energy loss in the target and the effect of Bevatron beam dynamics. The center of each plateau was selected for calibration purposes, but the slope indicates the magnitude of the uncertainties involved. This is the source of the large systematic uncertainty in the experimental results, and amounts to ± 15%.

Basically the accuracy with which the circulating beam can be measured is limited by the knowledge of three parameters: the length and the capacity of the electrostatic induction electrode and the shape of the rf structure of the Bevatron beam. In this case the uncertainty in the circulating beam was about ± 5%.

A correction must be made for multiple traversals in the lip during the clipper calibration experiment. The effective target thickness as seen by the monitor telescope was increased by this effect. For measuring the necessary correction the lip was made of plastic scintillator, as was the upstream surface of the target proper. A measure of the relative activity induced by the C^{12} (ppn) C^{11} reaction in the lip and on the edge of the target itself gives directly the number of traversals in the lip per single traversal of the target. This number was found to be about two at each energy.

II. RESULTS

A. Cross Sections

Measured differential cross sections are listed in Table I. As a result of recalibration of the circulating beam monitor, the corresponding values given earlier[8] should be lowered by about 9%. The total elastic cross sections may be obtained by integrating the differential spectra. In this procedure it is convenient to use a value for the forward-scattering cross section obtained by interpolation and extrapolation from the total cross-section measurements by other groups.[1,5,6] We set

$$\left(\frac{d\sigma}{d\Omega}\right)_0 = \left(\frac{k\sigma_T}{4\pi}\right)^2 , \qquad (3)$$

where k is the wave number of one of the interacting protons in center of mass, σ_T is the measured total cross section, and $\left(\frac{d\sigma}{d\Omega}\right)_0$ is the differential cross section at zero degrees. More precisely, this "optical" relation gives a lower limit on the forward-scattering cross section,[9] but use of the equality is valid for interactions dominated by inelastic processes. The integrated elastic cross sections obtained in this way are 17, 10, and 8 mb at 2.24, 4.40, and 6.15 Bev, respectively. Figure 7 shows the results of this experiment together with other measurements of the elastic and inelastic p-p cross sections in the energy range 0.5 to 6 Bev.

B. Uncertainties

The uncertainties in the cross-section measurements may be divided into two groups, systematic and random. The total effective random uncertainties are included in Table I. The expressed uncertainty in the center-of-mass angle is a reflection of about 1/4 inch uncertainty in the target position relative to the counters. The effect of this uncertainty is most serious at small angles and high energy, where the rate of change of cross section with angle is appreciable. The random uncertainty expressed in the cross-section measurements is made up of counting statistics, angular fluctuations due to target instability, variations in the average energy of the beam, and interpretation of the background subtraction as indicated in Fig. 5. The uncertainties due to counting statistics and background subtraction are important only at the larger angles, where the cross section is low. Target instability affects primarily

Table I

Differential cross sections for elastic p-p scattering. The uncertainties expressed are random only. In addition, a systematic uncertainty of ± 15% at each energy applies. Integrated cross sections are given in the text.

T (Bev)	θ_o (deg.)	θ_{cm} (deg.)	$\frac{d\sigma}{d\Omega}$ (mb/sterad)	statistics (%)	Total random uncertainty (%)
2.24	5	14.75±0.3	20.8	2.4	5.9
	8	23.6 ±0.3	11.0	1.8	5.4
	10	29.2 ±0.25	6.64	2.4	9.2
	15	44.0 ±0.26	1.12	2.0	8.7
	20	57.6 ±0.33	0.428	3.1	14
	25	70.3 ±0.4	0.255	3.0	13.4
	35	93.5 ±0.4	0.1455	3.3	19.1
4.40	3	10.6 ±0.4	20.5	1.7	5.3
	4	14.2 ±0.4	18.3	1.2	7.8
	5	17.5 ±0.4	12.73	1.2	7.1
	6	21.3 ±0.4	6.01	1.8	8.6
	7	24.5 ±0.4	2.96	2.1	11.0
	8	28.5 ±0.4	1.99	6.6	11.7
	10	37.4 ±0.4	0.473	7.1	13.4
	15	53.2 ±0.4	0.100	11.1	29
	20	69.0 ±0.4	0.0382	21	41
6.15	1.9	7.6 ±0.4	27.7	2.25	10.2
	3	11.6 ±0.4	24.6	3.1	9.0
	4	15.2 ±0.4	10.1	3.7	13.0
	5	20.0 ±0.4	5.51	3.5	20
	5	20.8 ±0.4	3.06	7.8	23
	6	23.6 ±0.4	1.31	15.6	24
	7	27.6 ±0.4	0.651	7.0	45

the small-angle measurements. Fluctuations in the average beam energy affect the counter alignment through the (relativistic) dependence of the included angle upon bombarding energy.

In addition to the random uncertainties given in Table I and discussed above, there is considerable systematic uncertainty at each energy. This arises primarily from the uncertainty in the number of multiple and partial traversals of the thick target used in the absolute calibration experiment. In addition there is about 5% uncertainty in the calibration of the circulating beam monitor, as well as smaller uncertainties appearing in corrections applied for self-absorption of the "thick" target used in calibration and for electronic counting inefficiencies. The total systematic uncertainty is about ± 15% at each energy. It is apparent that measurements at different energies are not wholly independent with respect to this uncertainty.

III. OPTICAL MODEL

We have attempted to interpret the experimental results at each energy in terms of the optical model developed by Fernbach, Serber, and Taylor.[10] A region of interaction between two particles may be described in terms of a complex index of refraction, with the real and imaginary parts producing phase shift and attenuation, respectively, of the incident plane wave of the colliding particles. If the index changes only slightly over the distance of a single wavelength (W. K. B. approximation), then the incident wave may be considered as a series of rays whose complex phase shift in traversing the region of interaction is a function of position. This is approximately equivalent to the condition that a large number of partial waves take part in the interaction. Alteration of the incident plane wave implies elastic scattering, for which the amplitude is given by

$$f(\theta) = k \int_0^\infty (1 - ae^{i\phi}) J_0 (k\rho \sin \theta) \cdot \rho d\rho \,, \qquad (4)$$

where θ is the scattering angle; ρ is the projected distance from the center of the interaction measured on a plane perpendicular to the direction of one of the incident particles; a and ϕ are the amplitude and phase shift, respectively, of a transmitted wave of unit initial amplitude and zero initial phase shift. The a and ϕ are, in general, functions of ρ. From Fernbach et al.[10] the elastic cross section is given by

$$\sigma_e = 2\pi \int_0^\infty \left|(1 - ae^{i\phi})\right|^2 \rho d\rho \,. \qquad (5)$$

and the absorption cross section by

$$\sigma_a = 2\pi \int_0^\infty (1 - a^2)\, \rho d\rho \,. \qquad (6)$$

For the p-p interaction, this model is complicated by the presence of spin and the identity of the interacting particles. Even and odd orbitals, corresponding to the singlet and triplet spin states, respectively, do not interfere. Analysis of the angular distribution in terms of Eq. (4) could be carried through as a superposition of noninterfering singlet and triplet distributions. If the spin forces are unimportant, however, and if the number of contributing partial waves is large, the angular distributions from the singlet and triplet spin states are identical. We have neglected any differences in the singlet and triplet states in the interest of simplicity and in order to minimize the number of free parameters used in fitting the experimental results. Spin-orbit forces, which are important in the lower-energy p-p interaction,[11] have been neglected. Some justification for this is found in the detailed phase-shift analysis by Rarita[4] of the results of Smith, McReynolds, and Snow at 1 Bev.[2] For the present we neglect also incoherent elastic scattering.

From the form of Eq. (4) the angular distribution is a function only of $k \sin\theta$ for a given radial dependence of a and ϕ. Figure 8 suggests that, to a fair approximation, the radial "form factor" of the interaction may be independent of energy.

From References 1 and 2 the value of σ_a is 26 mb for energies near 2 Bev. From the recent Berkeley cloud chamber results we have $\sigma_a = 25.6 \pm 3$ mb at 5.3 Bev.[6] For simplicity we substitute $\sigma_a = 26$ mb in Eq. (6) at each energy, 2.24, 4.40, and 6.15 Bev.

In order to obtain σ_e at each energy we have integrated the differential cross section over all solid angle, using the relationship between forward scattering and total cross section as an aid in extrapolating to zero angle. Since we have $f(0) \geq \frac{k\sigma_T}{4\pi}$, the total cross section, $\sigma_T = \sigma_e + \sigma_a$, gives a lower limit to the forward-scattering amplitude. We find $\sigma_e = 17 \pm 3$, 10 ± 2, and 8 ± 2 mb, at 2.24, 4.40, and 6.15 Bev, respectively. These values restrict a and ϕ through Eq. (5).

The analytic forms of functions a and ϕ were chosen in such a way as to make calculations according to Eq. (4) relatively easy. Several models were tried.

(a) Purely absorbing disk. $\phi = 0$; a = const for $0 \leq \rho < R$; a = 0 for $\rho > R$. The angular distributions calculated from Eq. (4) are illustrated by the dotted curves of Figs. 9, 10, and 11.
At 2.24 Bev, $R = 0.931 \cdot 10^{-13}$ cm, a = 0.209;
at 4.40 Bev, $R = 1.015 \cdot 10^{-13}$ cm, a = 0.444;
at 6.15 Bev, $R = 1.072 \cdot 10^{-13}$ cm, a = 0.530.

(b) Absorbing disk with short-range phase shift.
ϕ = const for $0 \leq \rho < R_1$; $\phi = 0$ for $\rho > R_1$; a = const for $0 \leq \rho < R_2$, a = 0 for $\rho > R_2$. $R_1 = 0.6 \cdot 10^{-13}$ cm, $R_2 = 1.2 \cdot 10^{-13}$ cm, a = 0.653 at all energies; at 2.24 Bev, $\phi = 1.35$; at 4.40 Bev, $\phi = 0.810$; at 6.15 Bev, $\phi = 0.600$. This is illustrated by the dashed curves of Figs. 9, 10, and 11.

(c) Tapered absorption with short-range phase shift.
$(1 - a) = A(1 - (\rho/R_2)^2)$; ϕ = const for $0 \leq \rho < R_1$; $\phi = 0$ for $\rho > R_1$; A = const for $\rho < R_2$; A = 0 for $\rho > R_2$. $R_2 = 1.41 \cdot 10^{-13}$ cm; A = 0.50 at all energies. At 2.24 Bev, $R_1 = 0.564 \cdot 10^{-13}$ cm, $\phi = 1.67$;
at 4.40 Bev, $R_1 = 0.521 \cdot 10^{-13}$ cm, $\phi = 1.08$;
at 6.15 Bev, $R_1 = 0.494 \cdot 10^{-13}$ cm; $\phi = 0.859$. This is illustrated by the solid curves of Figs. 9, 10, and 11.

The pronounced diffraction effects predicted by model (a) may be softened somewhat if the strength of the absorption is tapered with ρ. However, because of the high sensitivity of the elastic scattering cross section to the opacity, $(1 - a^2)$, in the region of interaction, the amount of tapering that can be tolerated in fitting σ_e and σ_a at 2.24 and 4.40 Bev is limited. At 6.15 Bev, on the other hand, considerable tapering is possible, since σ_e is much smaller than σ_a. The gaussian taper used by Belen'kii[12] in describing the π^- - p interaction at 1.4 Bev[13] is convenient for calculation, and can be used to describe the 6.15-Bev results.

At small angles the experimental results are fitted well by model (a). At 2.24 Bev, R = 0.931, in agreement with the cloud-chamber measurements at the Cosmotron.[5]

Introduction of a short-range potential-like interaction in models (b) and (c) brings the large-angle scattering at 2.24 and 4.40 Bev into much better agreement with experiment. The fit at large angles is rather sensitive to the

value of R_1. Tapering the region of interaction produces a smoother angular distribution. With the addition of a potential-like core, more tapering is possible; and with model (c) a smooth angular distribution can be obtained even at rather large angles. The measurements by Smith et al.[2] are also in fair agreement with model (c).

The parameters involved in model (c) may be made approximately energy-independent, but some latitude exists in the choice of numerical values. It is found that R_2 may be changed by about ± 10% from the value given, provided R_1 is changed in proportion; ϕ and A must be altered correspondingly to satisfy Eqs. (11) and (12). The amount of real phase shift ϕ required to fit the experimental cross sections decreases somewhat more rapidly than would be expected from a potential that is energy-independent in the nonrelativistic sense. Relativistic effects are probably very important, however, especially at the higher energies.

The sign of ϕ is not given by the experimental results. That is, we do not know whether the potential-like interaction is attractive or repulsive. Observation of the effects of interference with the Coulomb field could give the sign of ϕ, but measurements must be made at smaller angles than were feasible in this experiment. The strength of potential needed to produce the observed ϕ can be estimated by a semirelativistic calculation and is on the order of a few hundred Mev. Since with the present simplified model we can determine only an effective potential averaged over several wavelengths, it is possible that the nucleon-nucleon forces at small distances are quite singular. Several such models with this characteristic have been proposed to explain proton-proton elastic scattering in the region of a few hundred Mev.[14,15] Recently a relativistic model of the nucleon-nucleon and nucleon-antinucleon interactions has been proposed by Duerr and Teller.[16] Very strong short-range forces are predicated in both interactions.

Neither the experimental results nor the optical model employed in fitting them are sufficiently accurate to give the detailed shape of the radial dependence of ϕ and a. We may, however, define a mean-square projected radius for the attenuation and phase-shift interactions proposed; i.e., let

$$\overline{\rho_1^2} = \left(\int_0^\infty \phi\rho^3\, d\rho\right) \Big/ \int_0^\infty \phi\rho d\rho \,. \qquad (7)$$

$$\overline{\rho_2^2} = \left(\int_0^\infty (1 - a^2)\, \rho^3\, d\rho \right) / \left(\int_0^\infty (1 - a^2)\, \rho d\rho \right) . \qquad (8)$$

From model (c) we obtain $(\overline{\rho_1^2})^{1/2} \approx 0.37 \cdot 10^{-13}$ cm; $(\overline{\rho_2^2}) \approx 0.80 \cdot 10^{-13}$ cm. Model (b) gives comparable values.

Assuming that the interaction is spherically symmetrical, we may calculate the mean-square radii for the phase-shifting and absorptive interaction, e.g.,

$$\overline{r_{1,2}^2} \approx 3/2\ \overline{\rho_{1,2}^2} \text{ or } (\overline{r_1^2})^{1/2} \approx 0.45 \cdot 10^{-13} \text{ cm}, \quad (\overline{r_2^2})^{1/2} \approx 0.98 \cdot 10^{-13} \text{ cm} .$$

It is of some interest to compare these values with the Stanford measurements of the electromagnetic size of the nucleon. For a number of assumed shapes for the distribution of the charge on the nucleon, Chambers and Hofstadter[17] obtain $(\overline{r_e^2})^{1/2} \approx 0.77 \pm 0.10 \cdot 10^{-13}$ cm, intermediate between the values we obtain for $(\overline{r_1^2})^{1/2}$ and $(\overline{r_2^2})^{1/2}$.

IV. CONCLUSIONS

The high-energy elastic proton-proton scattering is at least partly a diffraction effect arising from the inelastic processes that can occur. Using the form of the optical model due to Fernbach, Serber, and Taylor,[10] we can fit the small-angle scattering with a variety of models. The scattering at large angles is particularly sensitive to the model used, and a strong short-range potential-like interaction seems to account best for the observed distributions. Unfortunately the optical model is least accurate in describing the large-angle scattering, partly because the requirement that a large number of partial waves participate in the interaction is not well satisfied for the short-range interaction. In any case it seems to be impossible to account for the observed angular distributions on the basis of a purely absorptive interaction.

Other models that lead to considerable large-angle scattering have been proposed in connection with the experimental π^--p angular distributions. A "thermal" model can account for the small isotropic component of the π^--p scattering at 1.4 Bev.[13] In the "thermal" model the colliding particles are imagined to stick together for a time during which the phase becomes random with respect to the initial phase. The angular distribution of particles re-emitted elastically in this process is isotropic. Since the experimental p-p

angular distributions decrease rapidly with angle at all three energies at which measurements were made, the amount of incoherent scattering must be small.

A resonance in a particular angular-momentum state has been considered as a means of accounting both for the increase in the π^+-p cross section near 1.3 Bev,[18] and for the observed secondary maximum in the elastic π^--p angular distribution at 1 Bev.[19] The smooth angular distributions observed at all energies in the elastic p-p scattering, on the other hand, suggest that several partial waves, at least, are important in determining the large-angle scattering.

Because of the similarity of many of the inelastic processes that occur in the π-p and p-p interactions, it is worth comparing the corresponding experimental measurements in some more detail. As has been pointed out, the inelastic p-p cross section is a nearly constant 26 mb for energies from 1 to 5 Bev. The measurements by Walker et al.[19] and Eisberg et al.[13] taken with those by Cool et al.[18] give a similar value for the inelastic π^--p cross section at 1.0 and 1.4 Bev. In the 4- to 5-Bev range, Bandtel et al.[19] find that the total π^--p cross section is about 30 mb, while cloud-chamber measurements give $\sigma_a/\sigma_e = 3.8$ for the ratio of the inelastic to elastic π^--p cross section.[21] Apparently the inelastic cross sections for the π^--p and p-p interactions are about equal and are nearly energy-independent.

The elastic cross section for the π^--p as for the p-p interaction shows considerable energy dependence at energies above 1 Bev. Furthermore, the angular distributions at 1 and 1.4 Bev can be interpreted in terms of a core of strong interaction superimposed on a purely absorbing region of larger radius.[13, 19] At energies above 1 Bev the elastic π^--p cross section is smaller than the p-p at corresponding center-of-mass energies. This may indicate that the effective potential is relatively weaker for the π^--p interaction or that a large part of the potential is velocity-dependent and decreases at higher velocities.

Near equality of the π^--p and p-p elastic and inelastic cross sections does not in itself require detailed similarity in the interactions. The small-angle scattering can be fitted by a variety of optical models. On the other hand, more complete measurements of the large-angle scattering at high energies for both processes can give more detailed knowledge of the interactions, and of the structure of the particles themselves.

ACKNOWLEDGMENTS

The requirements on target and beam control during this experiment were particularly stringent. For their support in the operation of the Bevatron we are indebted to the crew under the direction of Dr. Edward J. Lofgren.

REFERENCES

1. Chen, Leavitt, and Shapiro, Phys. Rev. 103, 211 (1956). This article includes a summary of the lower-energy data.
2. Smith, McReynolds, and Snow, Phys. Rev. 97, 1186 (1955).
3. R. Serber and W. Rarita, Phys. Rev. 99, 629A (1953).
4. W. Rarita, Phys. Rev. 104, 221 (1956).
5. Fowler, Shutt, Thorndike, Whittemore, Cocconi, Hart, Block, Harth, Fowler, Garrison, and Morris, Phys. Rev. 103, 1489 (1956).
6. Wright, Saphir, Powell, Maenchen, and Fowler, Phys. Rev. 100, 1802A (1955);
   also Bull. Am. Phys. Soc. Series II, 1, 386 (1956), and private communication.
7. E. McMillan, Rev. Sci. Instr. 22, 117 (1951).
8. Cork, Wenzel, and Causey, Bull. Am. Phys. Soc. Series II, 1, 376 (1956).
9. H. A. Bethe and F. de Hoffman, Mesons and Fields, Vol. II (Row, Peterson, New York, 1950), 76.
10. Fernbach, Serber, and Taylor, Phys. Rev. 75, 1352 (1949).
11. Oxley, Cartwright, and Rouvina, Phys. Rev. 93, 806 (1954).
12. S. Z. Belen'kii, J. Exptl. Theoret. Phys. (USSR) 30, 983 (1956); Soviet Physics J. E. T. P. 3, 813 (1956).
13. Eisberg, Fowler, Lea, Shephard, Shutt, Thorndike, and Whittemore, Phys. Rev. 97, 797 (1955).
14. R. Jastrow, Phys. Rev. 81, 165 (1951).
15. H. A. Bethe and F. de Hoffman, Mesons and Fields, Vol. II (Row, Peterson, New York, 1950), 306.
16. H. Duerr and E. Teller, Phys. Rev. 101, 494 (1956); also H. Duerr, Phys. Rev. 103, 469 (1956).
17. E. Chambers and R. Hofstadter, Phys. Rev. 103, 1454 (1956).
18. Cool, Piccioni, and Clark, Phys. Rev. 103, 1082 (1956).
19. Walker, Hushfar, and Shephard, Phys. Rev. 104, 526 (1956).
20. Bandtel, Bostick, Moyer, Wallace, and Wilmer, Phys. Rev. 99, 673 (1955).
21. Maenchen, Powell, Saphir, and Wright, Phys. Rev. 99, 1619 (1955); also Maenchen, Fowler, Powell, and Wright, Bull. Am. Phys. Soc. Series II, 1, 386 (1956); and private communication.

FIGURE CAPTIONS

Fig. 1. Experimental arrangement. T and T' are alternate target locations; S_1 and S_2 are inside-radius scintillation counters on remote-controlled cart C; S_3 and S_4 are outside-radius scintillation counters; S_3' is alternate outside counter, which can be rotated.

Fig. 2. Targets. (a) is of carbon or polyethylene and is dropped on a single nylon thread. (b) and (c) are of polyethylene and require two threads for orientation. The lip and front surface of (c) are scintillators made of terphenyl-loaded polystyrene.

Fig. 3. Block diagram of electronics. S_1 ... S_6 are scintillation counters. C_1 and C_2 are identical fast-coincidence circuits; D_1, D_2, and D_3 are fast discriminators. C_3 is the coincidence circuit for the monitor telescope. The A's are Hewlett-Packard 460A distributed amplifiers. SC_1, SC_2, SC_3 are scalars.

Fig. 4. Angular spectrum of coincidence. $\theta_{lab} = 5^\circ$. The accidental coincidence rate is subtracted from each point before plotting. The differential cross section is obtained from the integral of the smooth curve above the background level.

Fig. 5. Angular spectrum, $\theta_{lab} = 3^\circ$.

Fig. 6. Monitor yield from thick target. Curves above "plateau" show calculated location at clipper azimuth of beam that has passed through target once. The indicated width is the calculated spread of the displaced beam due to multiple Coulomb scattering in the target. Values for the field-gradient index, $n = 0.6$ and $n = 0.4$, have been assumed in calculation of the solid and dashed curves, respectively.

Fig. 7. Experimental proton-proton cross sections as a function of proton bombarding energy. Solid squares are from this experiment; solid circles, Reference 1; solid triangles, Reference 2; open circles, Reference 5, solid diamond is from this experiment and Reference 6.

Fig. 8. Experimental p-p differential elastic scattering cross section. Here k_c is the center-of-mass wave number of each colliding particle in units of 10^{13} per cm λ. Differential cross sections are center-of-mass values. The indicated forward-scattering cross sections are lower limits obtained from the "optical" theorem with the help of the total cross sections given in References 1 and 6. Uncertainties are not shown.

Fig. 9. Experimental p-p differential elastic scattering cross section at 2.24 Bev. Indicated uncertainties are random only and do not include a 15% systematic uncertainty. Curves show fits according to several optical models: dotted curve, model (a); dashed curve, model (b); solid curve, model (c). Parameters for each model are given in the text. The abscissa is in units of 10^{13} per cm.

Fig. 10. Experimental p-p differential elastic scattering cross section at 4.40 Bev. Indicated uncertainties are random only and do not include a 15% systematic uncertainty. Curves show fits according to several optical models: dotted curve, model (a); dashed curve, model (b); solid curve, model (c). Parameters for each model are given in the text. The abscissa is in units of 10^{13} per cm.

Fig. 11. Experimental p-p differential elastic scattering cross section at 6.15 Bev. Indicated uncertainties are random only and do not include a 15% systematic uncertainty. Curves show fits according to several optical models: dotted curve, model (a); dashed curve, model (b); solid curve, model (c). Parameters for each model are given in text. The abscissa is in units of 10^{13} per cm.

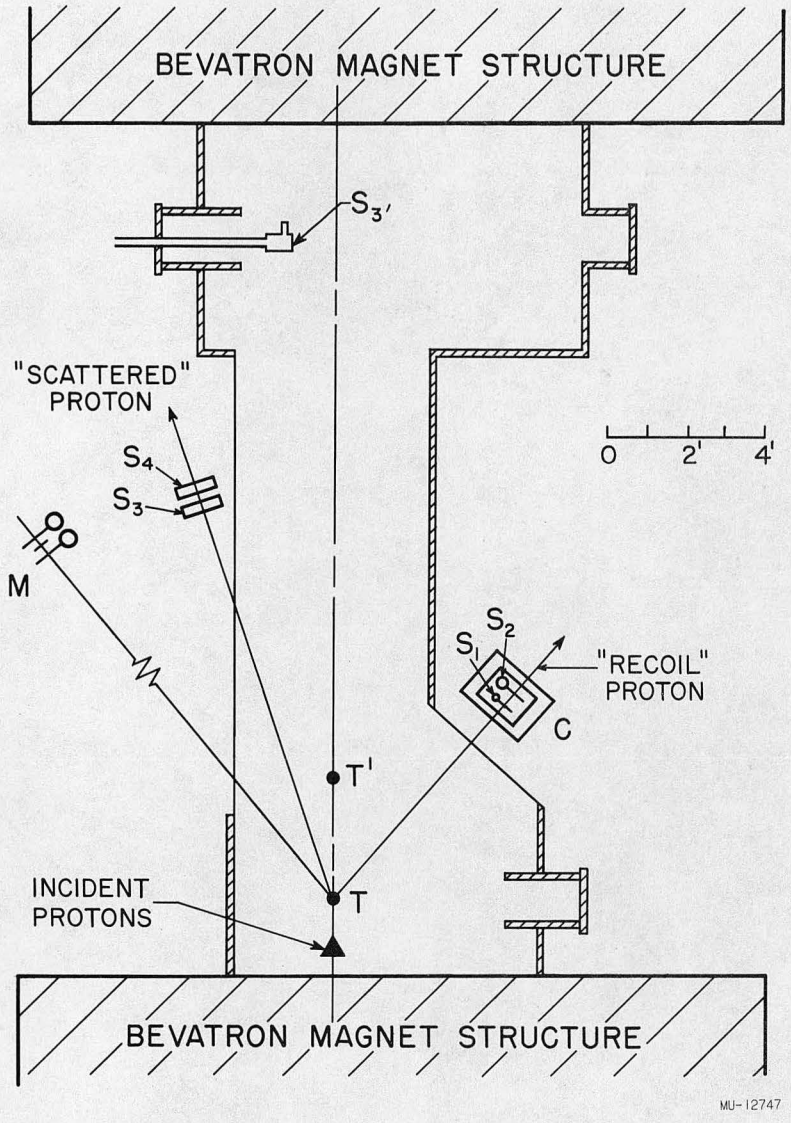
BEVATRON MAGNET STRUCTURE
S3'
"SCATTERED" PROTON
S4
S3
M
0 2' 4'
S2
S1
"RECOIL" PROTON
C
T'
INCIDENT PROTONS
T
BEVATRON MAGNET STRUCTURE
MU-12747

Fig. 1

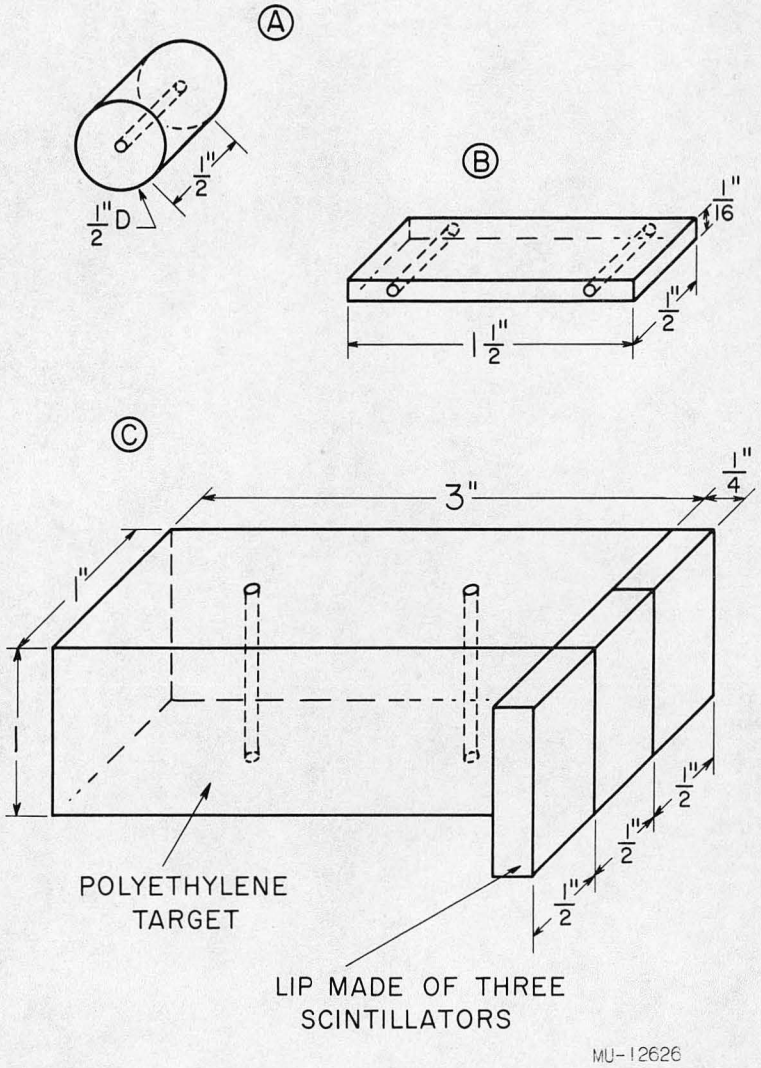
A
1/2" D
1/2"
B
1/16"
1/2"
1 1/2"
C
3"
1/4"
1"
1/2"
1/2"
1/2"
POLYETHYLENE TARGET
LIP MADE OF THREE SCINTILLATORS
MU-12626

Fig. 2

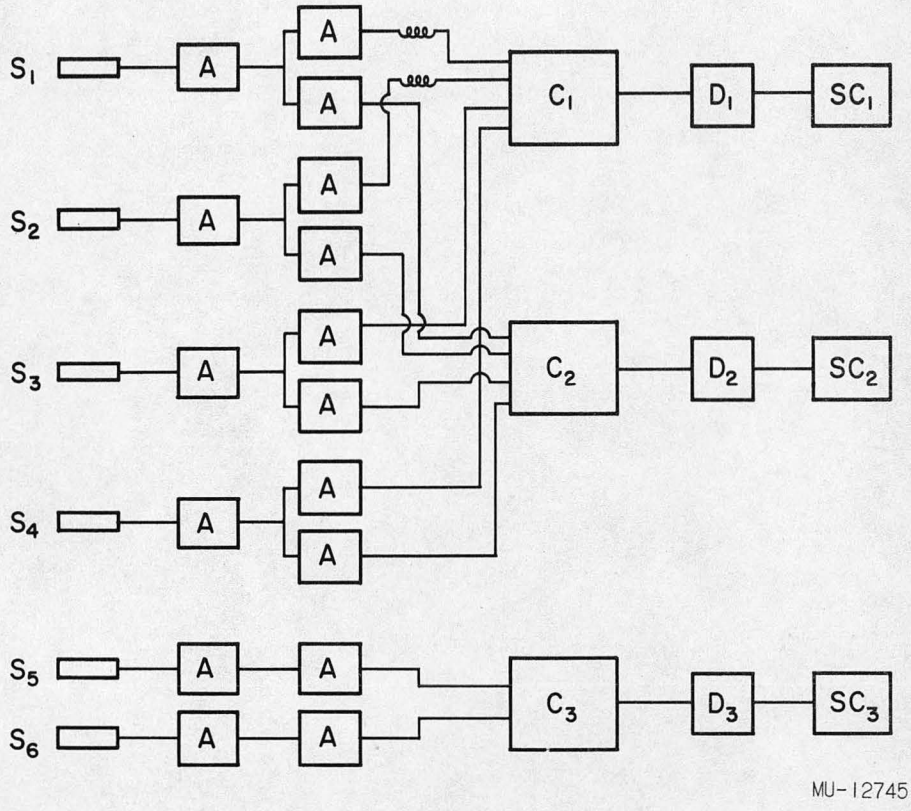

Fig. 3

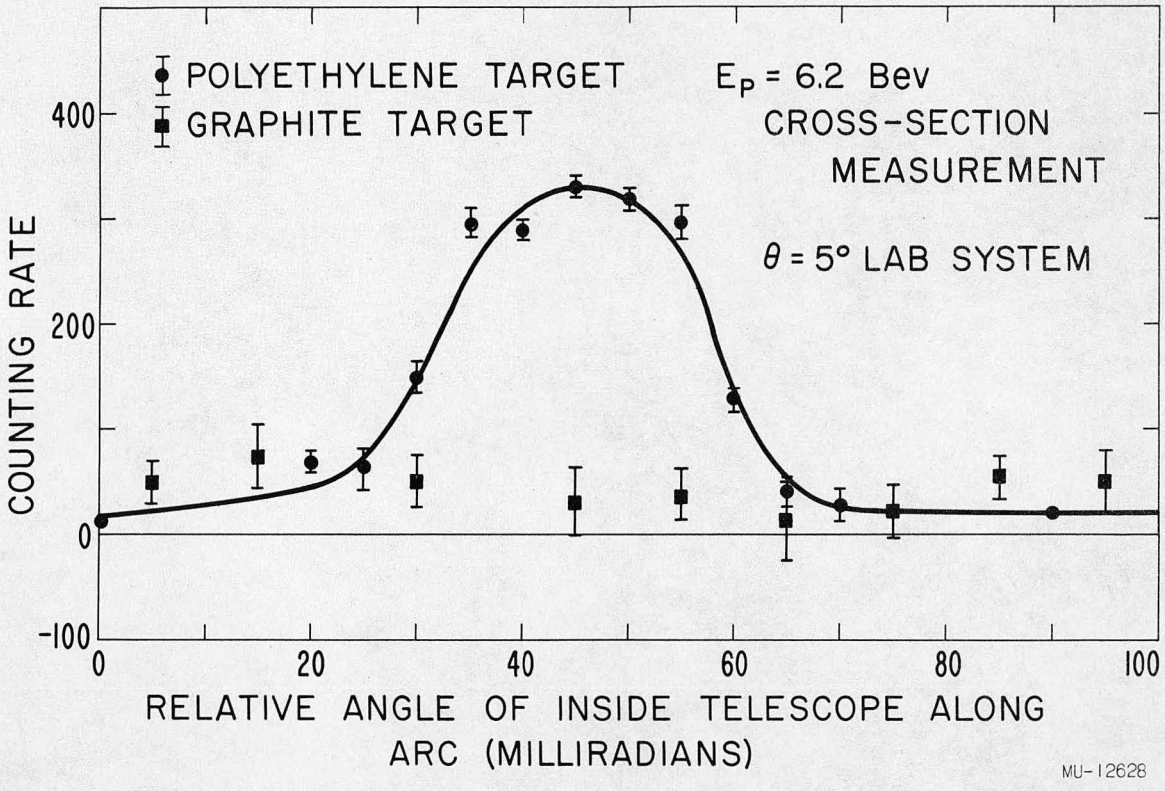
POLYETHYLENE TARGET
GRAPHITE TARGET
E_p = 6.2 Bev
CROSS-SECTION
MEASUREMENT
θ = 5° LAB SYSTEM
COUNTING RATE
400
200
0
-100
0
20
40
60
80
100
RELATIVE ANGLE OF INSIDE TELESCOPE ALONG
ARC (MILLIRADIANS)
MU-12628

Fig. 4

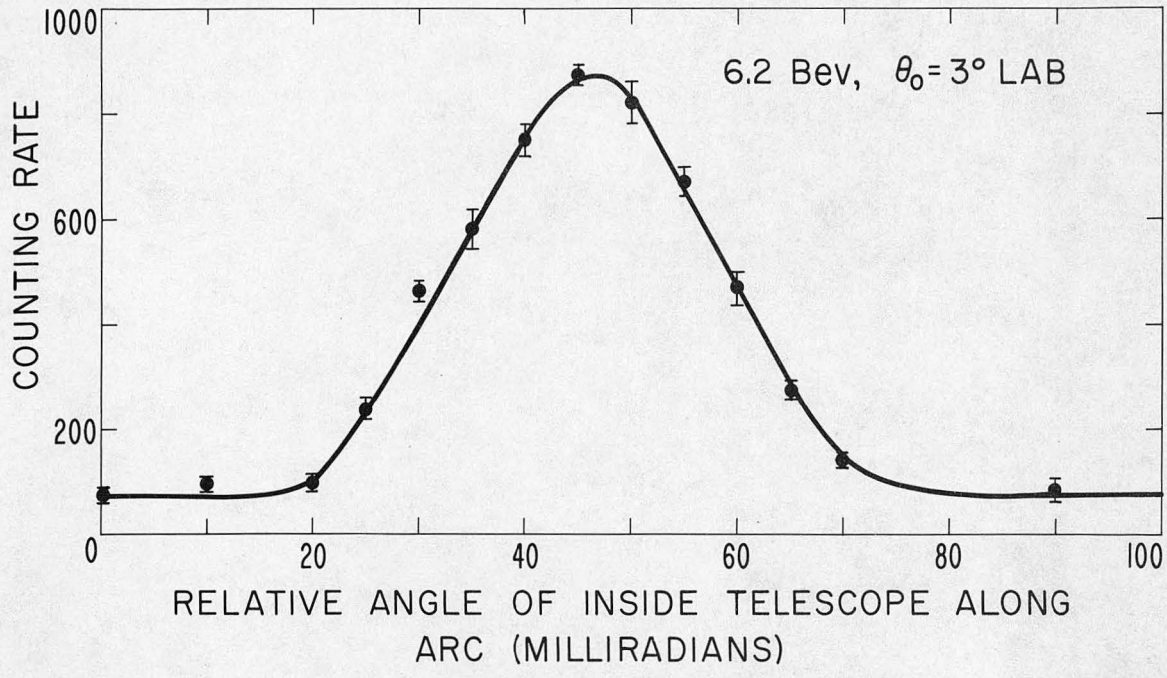
1000
600
200
0
COUNTING RATE
6.2 Bev, θ_0 = 3° LAB
20
40
60
80
100
RELATIVE ANGLE OF INSIDE TELESCOPE ALONG ARC (MILLIRADIANS)
MU-12627

Fig. 5

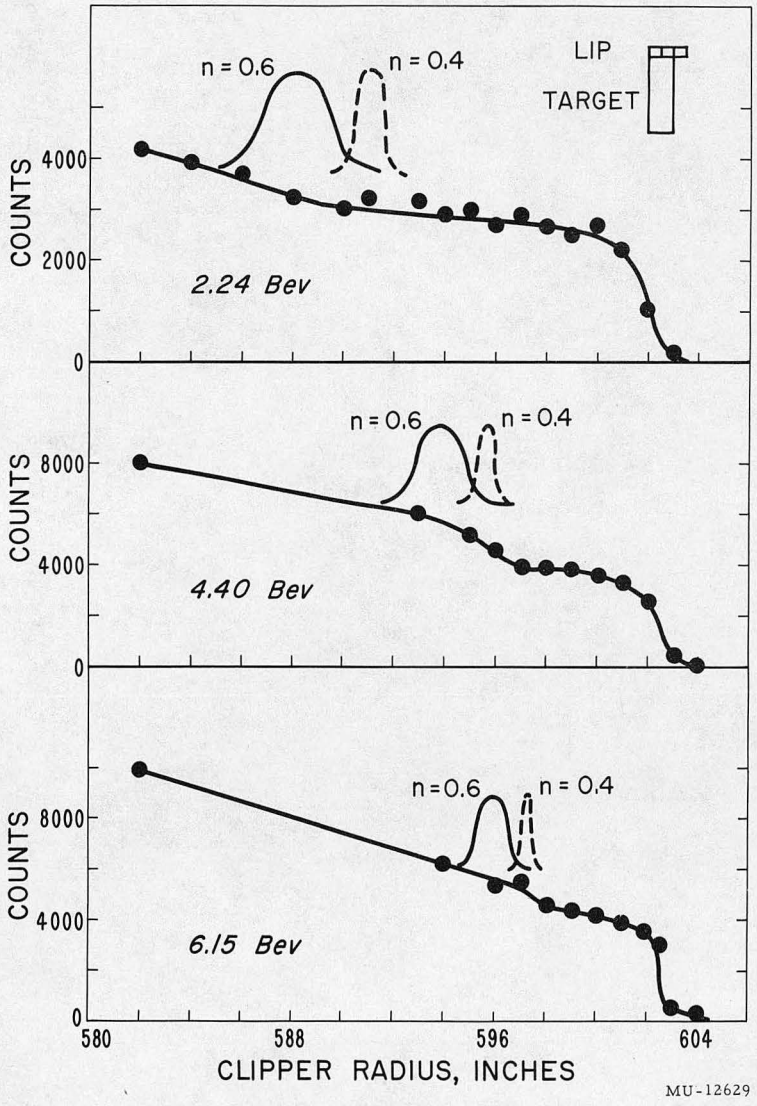
n = 0.6
n = 0.4
LIP
TARGET
COUNTS
4000
2000
0
2.24 Bev
n = 0.6
n = 0.4
COUNTS
8000
4000
0
4.40 Bev
n = 0.6
n = 0.4
COUNTS
8000
4000
0
6.15 Bev
580
588
596
604
CLIPPER RADIUS, INCHES
MU-12629

Fig. 6

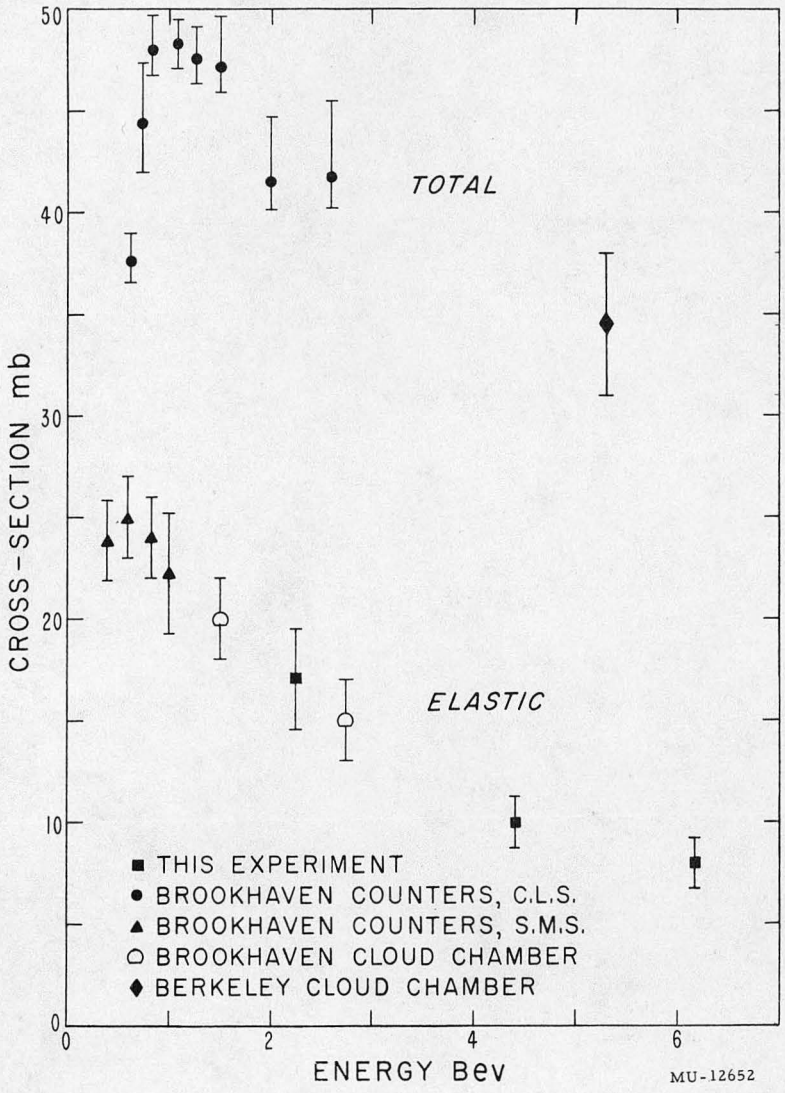
50
40
30
20
10
0
0
2
4
6
CROSS-SECTION mb
ENERGY Bev
TOTAL
ELASTIC
■ THIS EXPERIMENT
● BROOKHAVEN COUNTERS, C.L.S.
▲ BROOKHAVEN COUNTERS, S.M.S.
○ BROOKHAVEN CLOUD CHAMBER
♦ BERKELEY CLOUD CHAMBER
MU-12652

Fig. 7

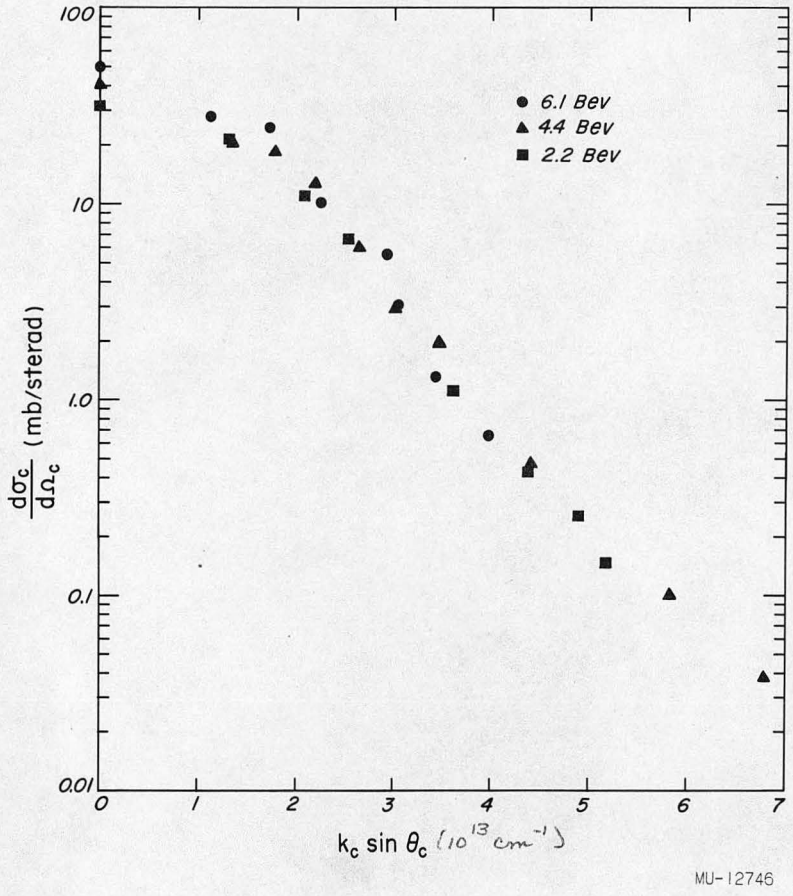
100
10
1.0
0.1
0.01
0
1
2
3
4
5
6
7
● 6.1 Bev
▲ 4.4 Bev
■ 2.2 Bev
$\frac{d\sigma_c}{d\Omega_c}$ (mb/sterad)
$k_c \sin \theta_c$ (10^{13} cm^{-1})
MU-12746

Fig. 8

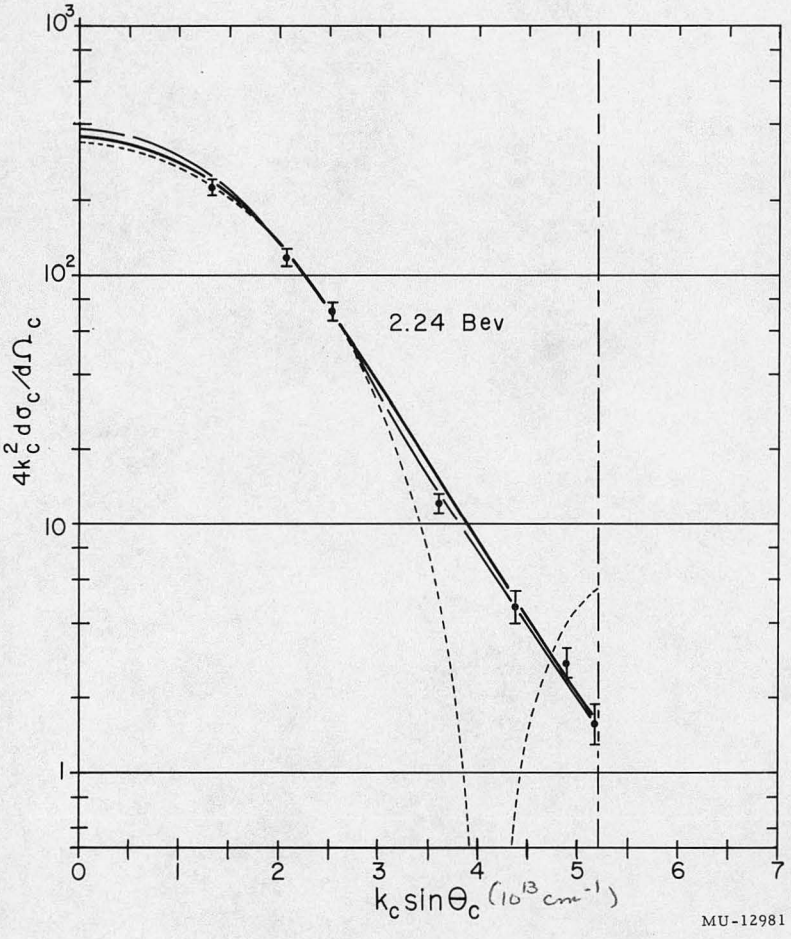
10^3
10^2
10
1
$4k_c^2 d\sigma_c/d\Omega_c$
2.24 Bev
0
1
2
3
4
5
6
7
$k_c \sin\theta_c$ (10^{13} cm^{-1})
MU-12981

Fig. 9

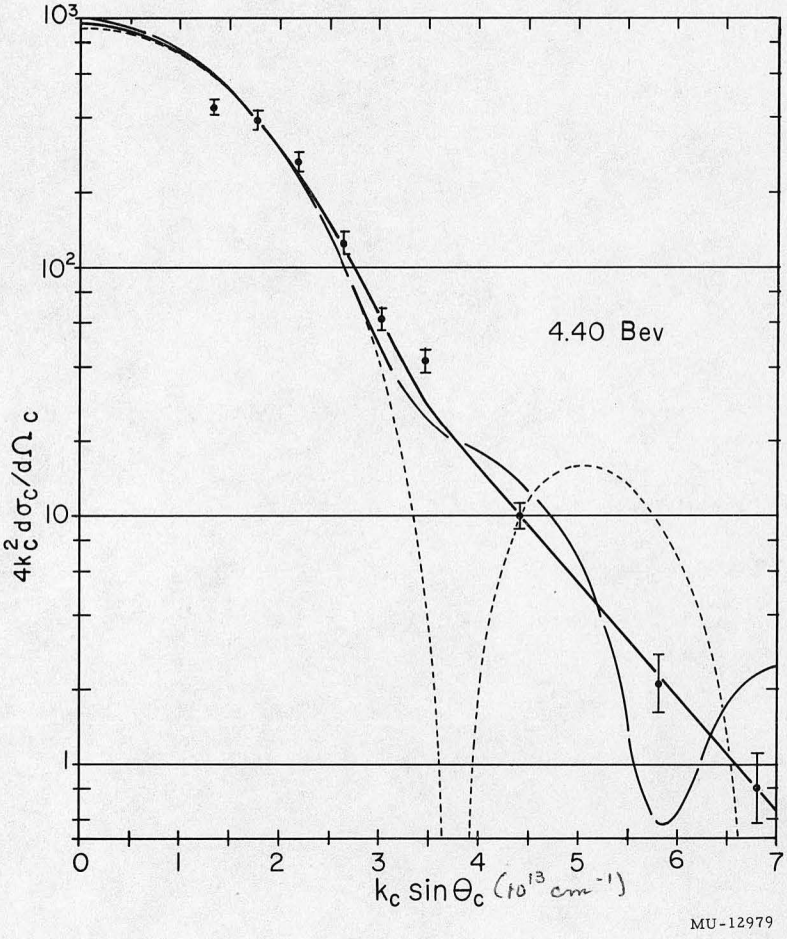
10^3
10^2
10
1
$4k_c^2 d\sigma_c/d\Omega_c$
4.40 Bev
0
1
2
3
4
5
6
7
$k_c \sin\theta_c$ (10^{13} cm^{-1})
MU-12979

Fig. 10

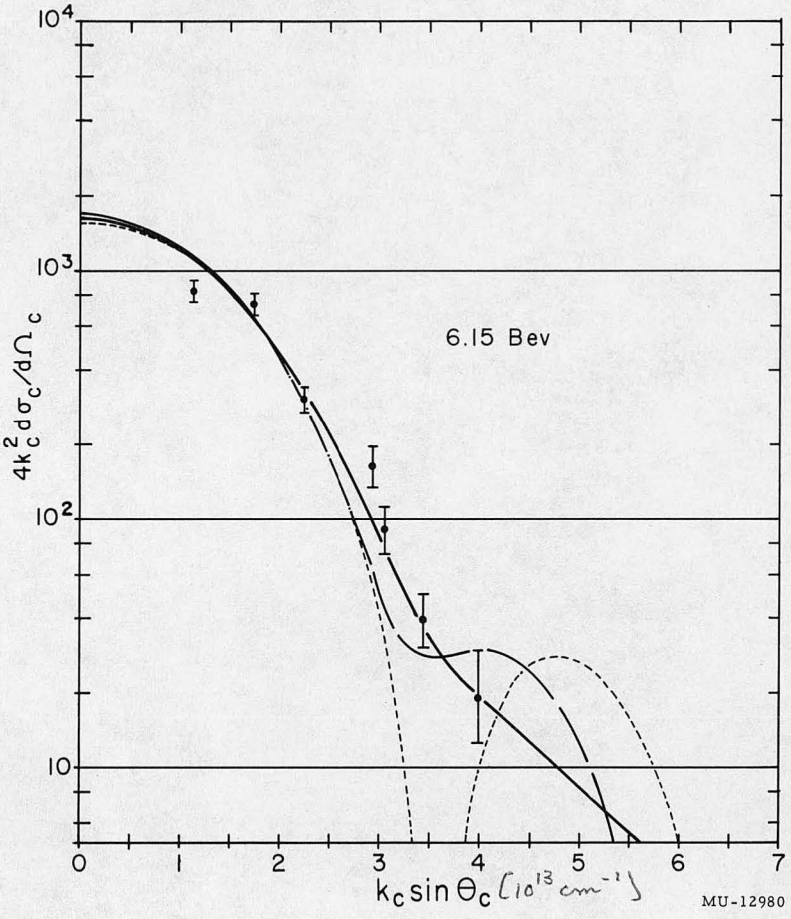
10^4
10^3
10^2
10
$4k_c^2 d\sigma_c/d\Omega_c$
6.15 Bev
0
1
2
3
4
5
6
7
$k_c \sin\theta_c$ [10^{13} cm^{-1}]
MU-12980

Fig. 11